Heliyon 9 (2023) e17811

Contents lists available at ScienceDirect

Heliyon

journal homepage: www.cell.com/heliyon

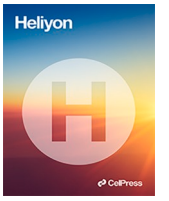

Atmospheric corrosion and impact toughness of steels: Case study in steels with and without galvanizing, exposed for 3 years in Rapa Nui Island

Rosa Vera [a,**], Bárbara Valverde [a], Elizabeth Olave [a], Rodrigo Sánchez [a], Andrés Díaz-Gómez [a], Lisa Muñoz [a], Paula Rojas [b,*]

[a] Institute of Chemistry, Faculty of Sciences, Pontificia Universidad Católica de Valparaiso, Av. Universidad 330, Placilla, Valparaíso, Chile
[b] Faculty of Engineering and Sciences, Universidad Adolfo Ibáñez, Diagonal Las Torres 2640, Santiago, Chile

ARTICLE INFO

Keywords:
atmospheric corrosion
Mild steel
Galvanized steel
Impact toughness
Marine environment

ABSTRACT

We studied atmospheric corrosion on Rapa Nui Island, using galvanized and non-galvanized SAE 1020 steel samples exposed on racks. We also added Charpy samples of both materials to directly determine the effect of corrosion rate on these materials' impact toughness. The results indicated a correlation between corrosion rate and toughness loss in the studied materials. In the corrosion study, we could also demonstrate the effect from increased insular population growth on contaminants which aid atmospheric corrosivity. Results showed that atmospheric SO_2 has tripled compared with similar corrosion studies done 20 years ago (Mapa Iberoamericano de Corrosión, MICAT), increasing corrosion rates. Our results show how human factors can influence changes in environmental variables that strengthen corrosion.

1. Introduction

Atmospheric corrosion is an important challenge for materials engineering. Climate change has accelerated corrosion in recent years, mainly due to higher temperatures and atmospheric CO_2 concentrations [1–6]. A recent study by Zhang et al. [7] on concrete and steel bridges built during the period 2000–2020 in 223 US counties determined the useful life of concrete and steel structures can decrease significantly depending on the climatic scenario, this effect being more than three times more significant in steel than in concrete in any scenario [7,8]. Research shows that for atmospheric corrosion, geographical location affects climate change impact levels, particularly in island and coastal areas. Chile is a tricontinental country [9], whose geographical location and coastal extension made it particularly sensitive to climatic changes in recent decades [10–15]. For this reason, and in light of increased national industrial development, a group of researchers developed an environmental corrosivity Map for Chile,[1] where the effect of the atmosphere on four metallic materials for industrial use was studied: carbon steel, galvanized steel, aluminum, and copper [16–19]. To create this map, 31 atmospheric testing stations were installed. The most distant stations from the American mainland were located in

* Corresponding author.
** Corresponding author.
E-mail addresses: rosa.vera@pucv.cl (R. Vera), barbara.valverdeolivares@gmail.com (B. Valverde), e.olave.n@gmail.com (E. Olave), rsgonzalez25@gmail.com (R. Sánchez), andresdiaz.qind@gmail.com (A. Díaz-Gómez), isa.munoz@pucv.cl (L. Muñoz), paula.rojas.s@uai.cl (P. Rojas).

[1] http://www.mapadecorrosionatmosfericadechile.cl/.

https://doi.org/10.1016/j.heliyon.2023.e17811
Received 5 January 2023; Received in revised form 27 June 2023; Accepted 28 June 2023
Available online 29 June 2023

Antarctica (King George Island, Fildes Peninsula, Scientific Base Professor Julio Escudero, (62° 12′ 57″ S–58° 57′ 35″ W) and in Oceania, on Rapa Nui or Easter Island (27° 07′ S–109° 22′ W).

Rapa Nui is one of the most isolated places on Earth. It is located in the Pacific Ocean, around 3700 km from the Chilean coast [20–22]. When constructing the environmental corrosivity Map for Chile, a station was installed on this island, specifically in the Marine Infantry Garrison of the Chilean Navy, located at Lat. 27.1565° S, Long. 109.4383° W, 22 m above sea level, and 500 m away from the sea. The island faces intense coastal storms because of its location. It has a Tropical Rainy climate (Af) according to the Köppen Geiger classification, with an average relative humidity of 77%, and an annual rainfall average of 1140 mm. Historically the rainiest month is May, and September is the driest. The yearly average temperature is 21 °C. Traditionally the average maximum temperature (23.3 °C.) occurs in March, and the average minimum temperature (17.9 °C.) occurs during August. Given that Rapa Nui is an isolated territory in the southeastern Pacific Ocean, far from South America, it is relevant to have information to develop specific adaptation strategies and reduce climate change impacts on the island. Coastal areas must adapt to boost their resilience to increasingly intense climate changes [8,23–26].

Between 1988 and 1994, an Ibero-American study carried out in 14 countries [27,28] included the island with a station [29]. Some of the data collected in this time will be compared with the data obtained more than 20 years later in this study, and in another location within the island. This research has also been carried out in many other island localities. Table 1 summarizes the research carried out regarding atmospheric corrosion on different islands, with their respective references [6,30–38].

Metals and metal alloys undergo atmospheric corrosion when their exposed surfaces become wet. The nature and rate of the attack depend on the electrolyte properties deposited on the surface, particularly concerning the level and type of gaseous and particulate pollutants in the atmosphere and the duration of their action on the metal surface [38]. Contaminants which primarily affect metals' corrosion kinetics are SO_2 and the anion Cl^- [38]. SO_2 is associated with fossil fuel combustion, making it common in industrial and urban areas. Rapa Nui does not meet these conditions because it is a relatively rural locality, which was also evaluated in this research. By contrast, the anion Cl^- is associated with marine environments, which is supposed to be more relevant on a small island like Rapa Nui. Contaminants and exposure time also determine the corrosion products in different exposed metals and alloys [30,38–42]. This research focused on galvanized and non-galvanized low-carbon steels, which are materials that react with atmospheric components forming hydroxides and oxides. In the case of steel, due to island conditions and the exposure times, we predicted the formation of Lepidocrocite γFeOOH, Goethite αFeOOH, Maghemite γFe_2O_3, and Magnetite Fe_3O_4 [43]. For galvanized steel, we predicted the products Zinc hydroxide $Zn(OH)_2$ and Zincite ZnO [44].

Materials' properties can alter due to the corrosion products formed. A relevant aspect of structural materials is the deterioration by atmospheric corrosion in mechanical properties [45]. Since this study focused on toughness, we used notched-bar impact testing of metallic materials by the Charpy (simple-beam) test, ASTM E23-98 with samples type V (Fig. 1a), [46]. Impact toughness is a relevant mechanical property when there is a possibility that the manufactured part needs to absorb energy from an impact. Steels and alloys generally exhibit two types of fracture behavior during impact tests, either ductile or brittle [47]. The amount of energy that metals and alloys can absorb depends on several factors such as composition, microstructure and temperature (Fig. 1b) [47–49]. Corrosion is a much less explored factor. Low carbon steels have high toughness at room temperature, but after galvanization, their toughness drops considerably due to the microstructural changes incorporated with the protection and the layers of Zn and intermetallic material [50]. However, galvanizing is widely used as a corrosion protection method due to its low cost and durability [51]; therefore, in this study it was considered for analysis and comparison with non-galvanized steel.

Table 1
Research on atmospheric corrosion in metallic materials carried out on islands around the world.

Island	Stations	Weather Köppen-Geiger	Exposed materials	Corrosion products	Ref
Canary Islands, Spain	39	BW, BS, Cs	Zinc, copper, aluminum, and galvanized steel	β–FeOOH, α–FeOOH, γ–FeOOH, and Fe_3O_4, Fe_2O_3	[32]
Cuban archipelago	6	Aw	Copper	$(Cu_2(OH)_3Cl$ $(Cu_3(SO_4)(OH)_4)$ $(Cu_4(SO_4)(OH)_6)$	[33]
Santa Cruz de Tenerife (Canary Islands, Spain)	35	BW, BS, Cs	Zinc	ZnO, $Zn_4CO_3(OH)_6$ H_2O, $Zn_5(OH)_8Cl_2$ H_2O, $NaZn_4Cl(OH)_6SO_4$ H_2O, $Zn_3O(SO_4)_2$, $Zn_4SO_4(OH)_6$	[31, 34]
Canary Islands, Spain	74	BW, BS, Cs	Carbon steel, copper, and zinc	$Zn_5Cl_2(OH)_8{\cdot}H_2O$ Cu_2O, $(CuCl_2{\cdot}3Cu(OH)_2$	[6]
Cuba	7	Aw	Carbon steel, copper, galvanized steel, and aluminum		[35]
Nansha Islands, China	1	Af	Copper	$Cu_2Cl(OH)_3$, Cu_2O	[36]
Nansha Islands, China	1	Af	Aluminum	Al_2O_3, $AlCl_3$, $Al(OH)_3$	[37]
Spratly Islands, Philippines, and Vietnam.	1	AM	Low-carbon steel	β–FeOOH, α–FeOOH, γ–FeOOH, and Fe_3O_4	[38]

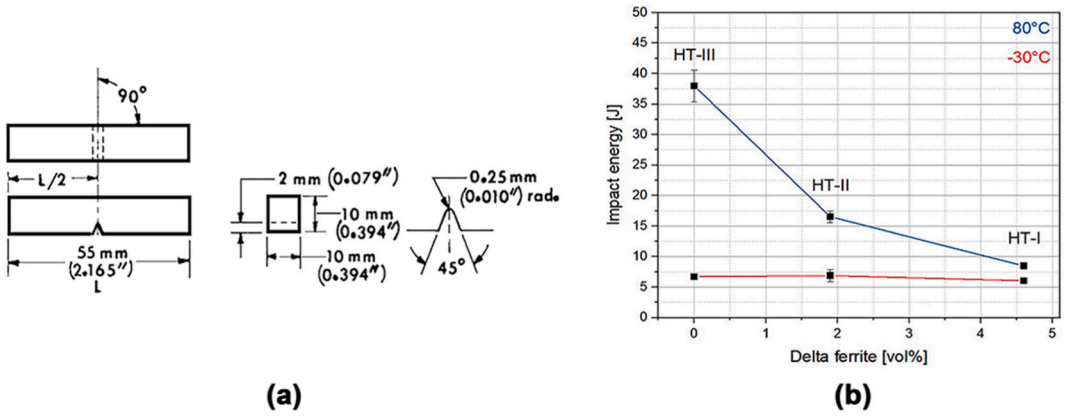

Fig. 1. (a) Charpy (Simple-Beam) impact test specimen, Type A [46], (b) Results from Charpy impact testing of different maraging steels, tested at 80 °C and – 30 °C [48].

2. Materials and methods

2.1. Atmospheric testing station, samples, and atmospheric data collection

Samples were exposed in racks in the same island area for the study, as shown in Fig. 2a [52]. For the steel frame, SAE 1020 carbon steel specimens (0.18–0.23%C, 0.28–0.65%Mn, 0.15–0.35%Si, <0.04%P, <0.05S) were exposed. In the galvanized steel frame, the same steel was used, but with a Zn surface layer 85 μm thick. The metal specimens' dimensions were 10 cm × 10 cm x 0.4 cm, all exposed at an angle of 45° in the frame and separated by plastic insulators according to ISO 9223 to 9226 standards [30,53–55]. Before atmospheric exposure, all specimens were degreased with acetone, washed with high-purity water, dried with cold air, and stored in a desiccator. Clean and dry samples were accurately measured and massed using the ASTM G1-03 standard [56]. Total exposure time was three years. In the same exposure area, specific devices were located to study contaminants, sulfates, and chlorides, (Fig. 2b and c). Deposition rates of atmospheric SO_2 (mg SO_2/m^2·day) and Cl^- (mg Cl^-/m^2·day) were calculated following ISO 9225 [54]. Meteorological data collection was carried out with the station at Latitude: −27.156556, Longitude: −109.438333, height: 22 m, and distance to the sea: 500 m. The data collected were: average annual temperature (T·°C), average annual relative humidity (RH) (%), amount of rainfall (mm), wind speed (m/s), and time of wetness (TOW). To calculate the latter point, we used the number of hours with RH ≥ 80% and T > 0 °C, expressed in hours per year.

2.2. Characterization of corrosion products

Material deterioration was evaluated every three months by measuring mass loss in triplicate (ASTM G50 [57]). The morphology of the attack was observed under a scanning electron microscope (SEM) using a Hitachi SU 3500 with a 410-M EDAX analyzer for elemental characterization [52].

To identify corrosion products, the X-ray diffraction technique was applied using a BRUKER instrument model D8 Advance, with Cu-Kα radiation and 40KV/30 mA graphite monochromator with a scanning range of 10–70°. Corrosion products were also analyzed using the Raman technique. The Carbon Steel and Galvanized Steel Raman spectra were obtained using a Raman Witec Alpha 300 confocal microscope system, equipped with a 785 nm wavelength laser and an electrically-cooled CCD camera. The signal was calibrated using the 520 cm^{-1} lines of a Si wafer and a 50X target. The resolution was set at 4 cm^{-1}, and ten scans were performed with an integration time of 1s. Spectra were recorded in the region 0 to 1700 cm^{-1}. An extra post-corrosion characterization was not performed, since it was not necessary to determine the corrosion rate.

2.3. Electrochemical measurements

The protective nature of the corrosion products formed on the materials in the environment was evaluated by performing anodic polarization curves in a solution of 0.1 M Na_2SO_4 at 25 °C with a scanning speed of 0.5 mV s^{-1}, using an Autolab Potentiostat model 302A, with a reference electrode of saturated calomel and a platinum wire counter-electrode. To determine the corrosion rate determination, the arithmetic average of three measurements was used [52].

2.4. Toughness measurements

Toughness tests were carried out with a JB-S300 Instrumented Charpy Impact Testing Machine, with a capacity of 300 J and digital data readout. The sample dimensions used in the Charpy test were 55 mm × 2 mm x 2 mm. Conditions indicated in ASTM E23-98 [46] were considered. For the samples in this test and the corrosion test to have similar exposure conditions, the samples were hung out in

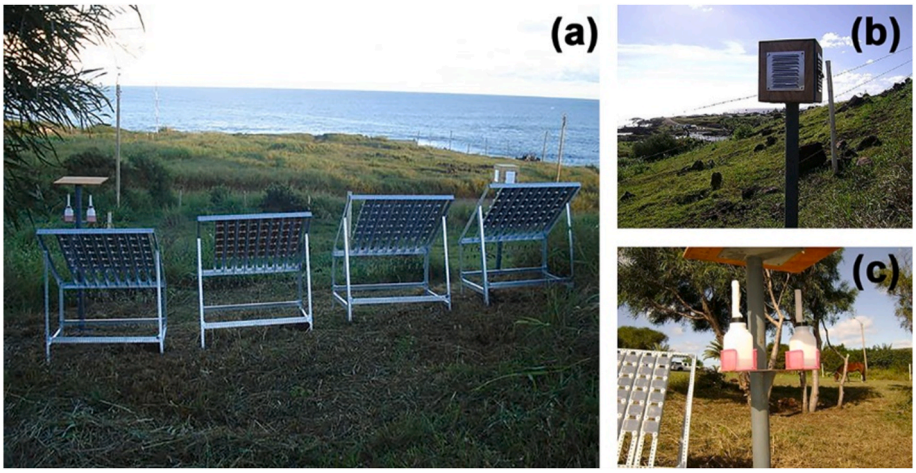

Fig. 2. (a) Atmospheric testing station in Rapa Nui, (b) Devices installed at the station to detect Sulfur dioxide, and (c) chloride deposition rates.

the racks and gathered at the same time periods as those in the rack (Fig. 3a–d).

3. Results and discussion

3.1. Atmospheric aggressivity factors

3.1.1. Temperature

According to the data measured over 36 months, a difference can be seen between the warmest months on the island between December and May, where temperatures varied between 28° and 16 °C (82–61 F), and the coldest temperatures between June and October, ranging between 23° and 12 °C (73–54 F) (Fig. 4). The average annual temperature for the three years of the study was 22 °C. Comparing this result with the MICAT study [58] done 20 years earlier, we can note an increase of 1.5 °C, since the average temperature in the former study was 20.5 °C.

3.1.2. Relative humidity and TOW

Relative humidity showed less variation than temperature. During the warmer months, relative humidity was 56–85%, while in the cooler months, it ranged between 54 and 90% (Fig. 5). Relative humidity in the MICAT study was 79%, i.e., relatively similar to that of the present study.

For time of wetness (TOW), the average during the three years of exposure was calculated at 3344 h/year. Therefore, according to ISO 9223, it is level τ_4 ($2500 < \tau < 5500$ h/a, Outdoor atmospheres in all climates). This value may be a little higher because on some days, the ambient temperature could facilitate evaporation, thus decreasing wetting. However, it would remain at the same level as the norm. According to the average value calculated for TOW, the metal surface is covered by a water film about 38% of the time in relation to the total number of hours per year (8760 h/year).

3.1.3. Pollutants

According to ISO 9223, an unpolluted atmosphere has a rating of S_0P_0, with very low chloride and SO_2 pollution, and a pure marine atmosphere would have a rating of S_1P_0, S_2P_0, S_3P_0 [30]. In this study, the results of the measured pollutants, chlorides, and sulfur dioxide (SO_2), are shown in Fig. 6(a) and (b). According to these data, in the case of chlorides, the first year of exposure reached an average of 53.04 mg m^{-2} day^{-1} for chloride (Cl^-) content; the second year saw an average of 51.13 mg m^{-2} day^{-1}; and the third year had an average of 48.37 mg m^{-2} day^{-1} [52]. These values all correspond to an $\mathbf{S_1}$ classification according to ISO 9223, because it is a marine environment. Average annual values were considered for comparisons with previous studies, since monthly variations appear in the case of atmospheric measurements, as the results indicate (Fig. 6a). On the other hand, the average environmental sulfur dioxide content for the first year was 1.89 mg m^{-2} day^{-1} (classification $\mathbf{P_0}$, rural atmosphere), in the second year 5.41 mg m^{-2} day^{-1} (classification $\mathbf{P_1}$, urban atmosphere), and in the third year 3.30 mg m^{-2} day^{-1} (classification $\mathbf{P_0}$, rural atmosphere) [52]. The presence of this pollutant is considered an anthropogenic effect due to the relationship between people and the consumption of fossil fuels, which generate SO2. With these changes, the significant population increase on the island may have affected its air pollutants, changing the environment from rural to urban. According to government data, between 2002 and 2015, the population of the island rose from 3791 to 6370 people [59], which meant the population almost doubled in under 15 years. Considering that during this timeframe, per capita greenhouse gas emissions in Chile[2] rose by 25%, this implied a significant increase in these gases on the island.

[2] https://ourworldindata.org/greenhouse-gas-emissions.

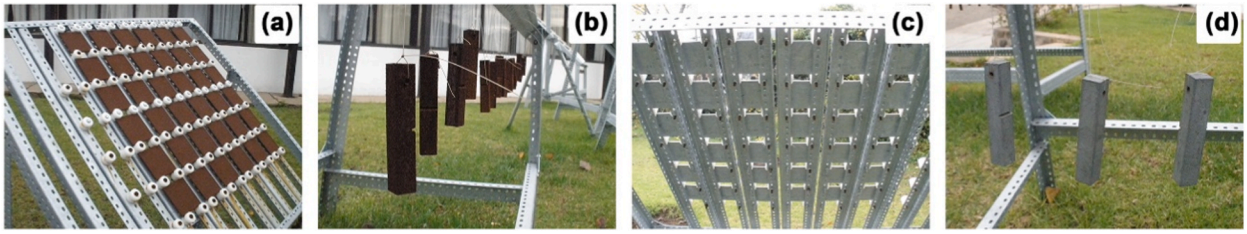

Fig. 3. Photographs of the racks used in the studies, showing the upper section of the rack, with the samples for corrosion rate (a and c), and the lower section, with hung samples for impact toughness tests (b and d).

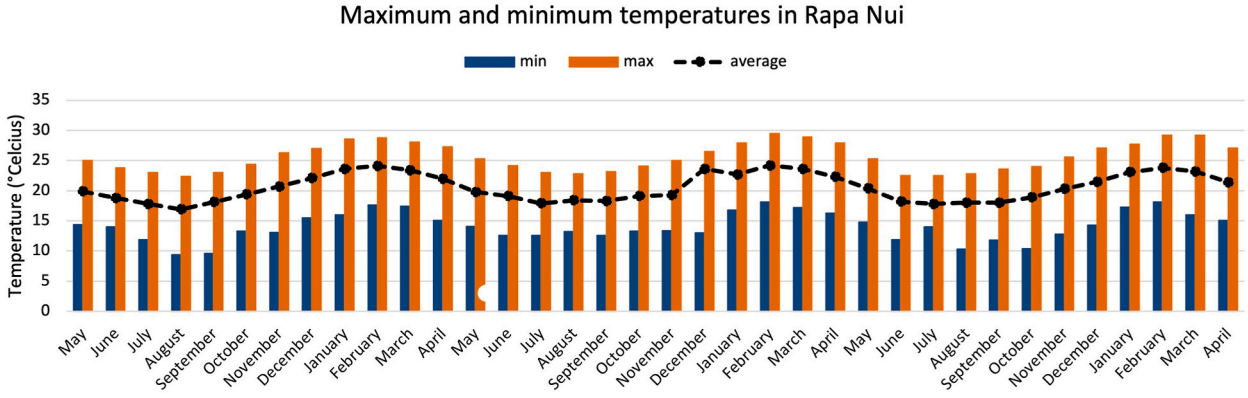

Fig. 4. Monthly maximum and minimum temperatures measured for three years in Rapa Nui.

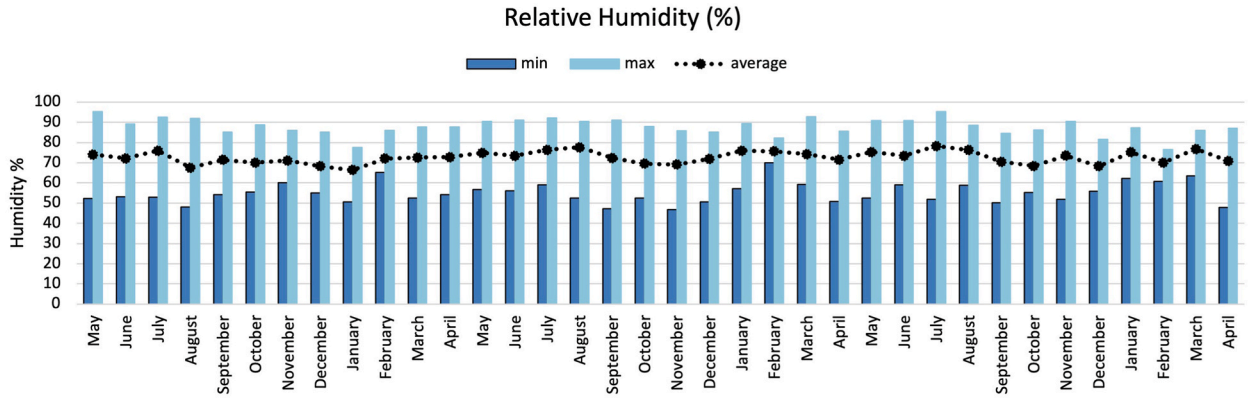

Fig. 5. Maximum and minimum monthly relative humidity measured for three years in Rapa Nui.

Considering the data obtained at the time of wetting, and the environmental content of chloride and sulfur dioxide, the category of environmental corrosivity was estimated according to ISO 9223. The results of the annual category appear in Table 2. The environmental corrosivity category was **C3,** which corresponds to average corrosivity usually presented in coastal areas with low chloride deposition or subtropical and tropical zones with low atmospheric pollution [52].

Twenty years ago, in the MICAT project [58], the samples were 300 m from the coastline and 0 m above sea level (m.a.s.l). The samples in our study were located 500 m from the coastline and 22 m.a.s.l. In this case, marine aerosols did not reach the samples as directly as in the MICAT project and could have shown C2 corrosion levels. Our results showed C3, though, which could be explained by the increase in atmospheric pollutants found in the current study.

3.2. Corrosion rates

3.2.1. Steel

Fig. 7a and b shows the variation in corrosion rate and loss of carbon steel thickness as a function of exposure time. These results

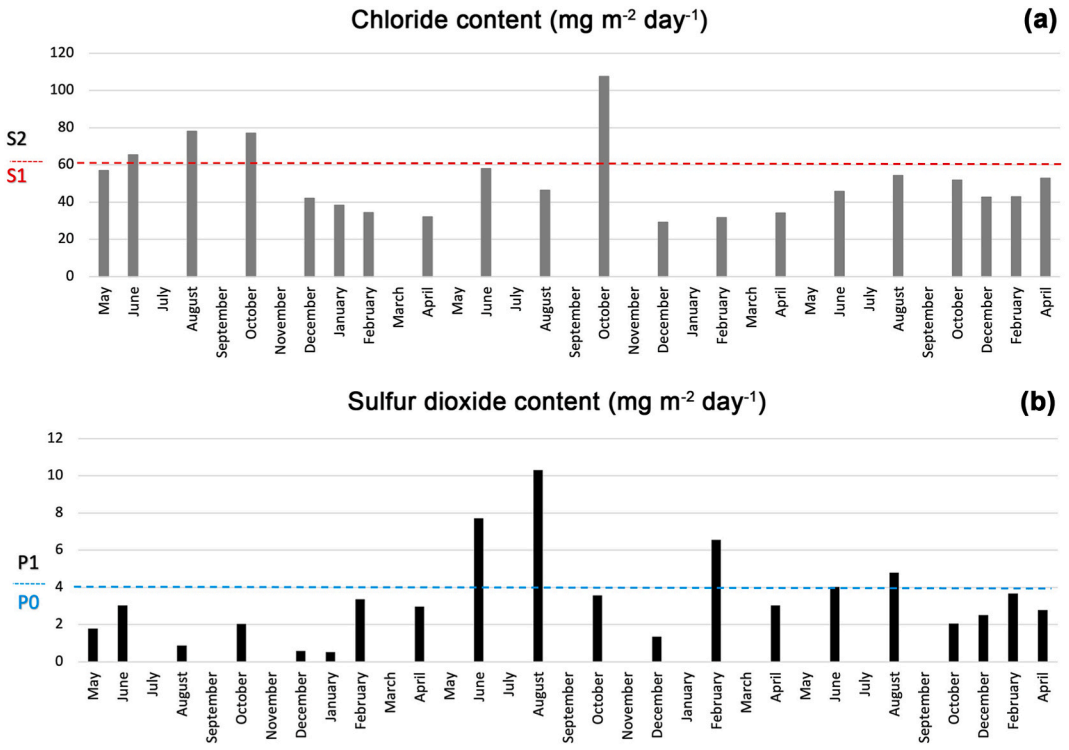

Fig. 6. Pollutants measured in Rapa Nui during different study months, (a) chloride content and (b) SO_2 content.

Table 2
Classification of environmental corrosivity categories on Rapa Nui.

Exposition (Year)	TOW (τ) (hour year $^{-1}$)	Chloride (S) (mg m^{-2} day^{-1})	Sulfur dioxide (P) (mg m^{-2} day^{-1})	Corrosiveness Category
1st	2616	53.04	1.89	τ4 S_1P_0/C3
2nd	3936	51.13	5.41	τ4 S_1P_1/C3
3rd	3480	48.37	3.30	τ4 S_1P_0/C3

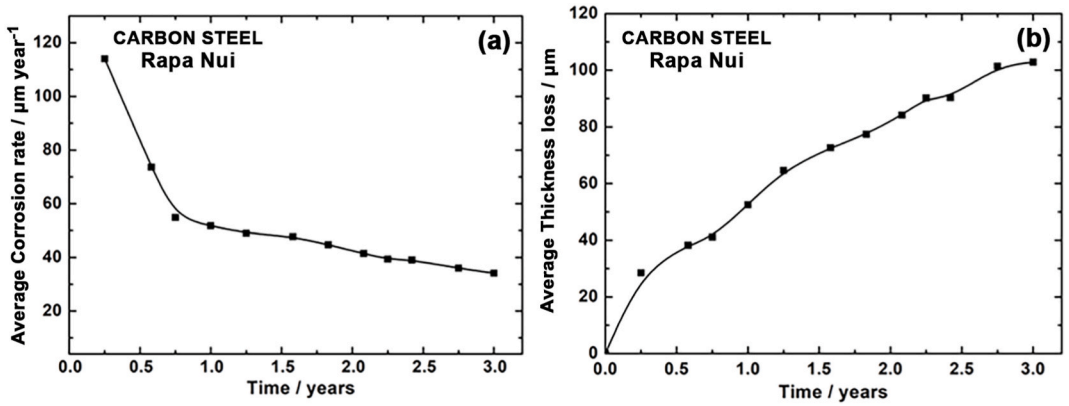

Fig. 7. Corrosion rate (a) and thickness loss (b) of carbon steel, as a function of exposure time.

indicate that as exposure time increases, the corrosion rate decreases, and thickness loss rises. Decrease in corrosion rate is due to the barrier effect provided by the corrosion products formed during exposure. This decrease depends on the type and protective nature of the corrosion products, which we analyze later.

The corrosion rate of steel, at one year of exposure, was **51.95 µm year^{-1}**. According to ISO 9223 [30], this value is classified into a

corrosivity category of **C4**.

In studies carried out on other islands (see Table 1), rates were 4.5 times [38] and up to 5.7 times [35] higher than the values determined for Rapa Nui. Consequently, in both cases, the category of corrosivity determined was CX. On the other hand, considering the deterioration of steel by a general corrosion process, the loss of steel thickness at three years of exposure is 102.8 μm, constituting 2.6% of the initial thickness of the material under the study conditions.

One of the most commonly used models to interpret the behavior of corrosion rate (or thickness loss) over time is given by the potential function $CR = A*\tau^n$ [60]. This model can also be represented through the bi-logarithmic model (equation (1)), and that has been previously reported by R. Vera et al. [52]:

$$\log_{10} CR = \log_{10} A + n * \log_{10} t \quad (1)$$

where:

- CR = corrosion magnitude (Thickness loss) of the metal or alloy at three years;
- A = corrosion measure (Thickness loss) at the first year of exposure (t = 1), and
- n = an indicator parameter of the physico-chemical behavior of the corrosion layer and its interactions with the atmosphere.
- t = metal exposure time, in years.

The function obtained for the carbon steel behavior under the study conditions in Rapa Nui appears in Equation (2), where n has a value close to 0.5. This corroborates that the corrosion mechanism is controlled by diffusion through the corrosion products that remain on the material, considering that average environmental chloride content in the area is low (50.85 mg m^{-2} d^{-1}).

$$CR_{CS} = 16.3268 \times t^{0.4877} R^2 = 98.92\% \quad (2)$$

Previous studies in Rapa Nui [58], which had conditions of temperature and relative humidity similar to the present work, but with lower measurements of SO_2 (1.15 mg m^{-2} day^{-1}) and chloride (Cl^-) (<50 mg m^{-2} day^{-1}), had an annual exposure corrosion rate for steel (SAE 1020) of between 30.0 and 32.8 μm $year^{-1}$ [29]. In the present study, the ambient SO_2 content was tripled (average 3.53 mg m^{-2} day^{-1}), and the average environmental chloride content was slightly higher (50.85 mg m^{-2} day^{-1}), ultimately causing a steel corrosion rate (SAE 1020) 1.5 times higher than that of Marco et al. [29]. These rates should not be compared without considering that the first study used steel with 0.7% C, while the second study used 0.2% C, affecting these materials' corrosion resistance. However, it is very relevant that the SO_2 content was higher, and this is an active cathode depolarizing agent 2600 times more soluble in water than oxygen (O_2), even if its content in the atmosphere is negligible. Since it is soluble in the electrolyte, it can have an oxidizing effect similar to oxygen itself, accelerating the cathode process, and increasing the corrosion rate of steel. SO_2 can be absorbed by rainwater as well, a condition that influences material corrosion rate. The amount of rainfall during the first year was 760.0 mm, while the second year saw 816.1 mm, and the third year had 1028.8 mm. Annual rainfall distribution was not homogeneous [52].

3.2.2. *Galvanized steel*

Fig. 8a and b shows variations in corrosion rate and thickness loss for galvanized steel as a function of exposure time. According to the data, the corrosion rate at all times was considerably lower than the same steel without protection. In fact, in the first year, the corrosion rate of galvanized steel represents 4% of that of ungalvanized steel, the second is 5%, and the third reaches 5.6%. What is comparable in both materials is that as exposure time increases, the corrosion rate decreases, and thickness loss increases.

The annual corrosion rate of exposed galvanized steel was 2.00 μm $year^{-1}$; according to ISO 9223, this value is classified as corrosivity **C3**. On the other hand, considering the deterioration of the galvanizing by a general corrosion process and that the average thickness of the galvanizing layer was 85 μm, the thickness loss of the layer after three years of exposure was approximately 8%. The

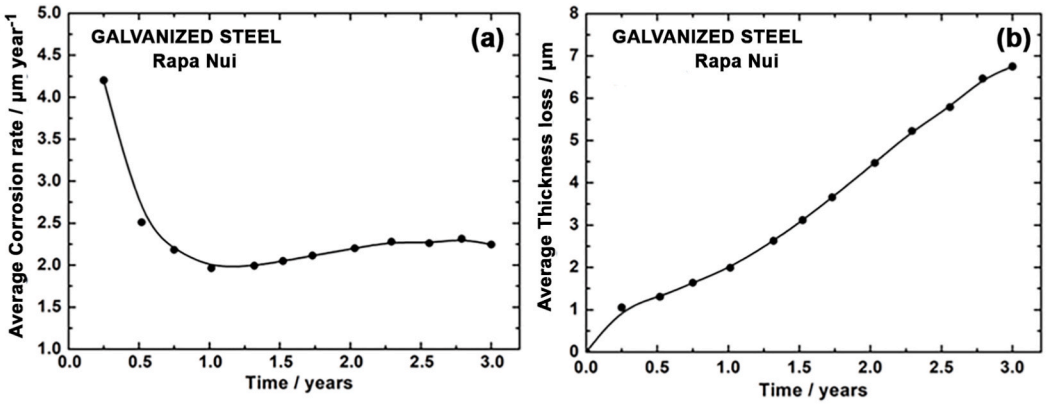

Fig. 8. Corrosion rate (a) and thickness loss (b) of galvanized steel, as a function of exposure time.

function obtained to explain the behavior of the thickness loss of galvanized steel during the exposure time in the study conditions appears in Equation (3). Since n has a value close to 1.0, it indicates an almost direct relationship between loss of thickness and exposure time. However, only the corrosivity category of C3 was reached as the category of environmental aggressiveness is $\tau_4S_1P_0$ (low average content of environmental chloride (Cl^-) in the area, which was 50.85 mg $m^{-2.}$ d^{-1}). The amount of rainfall must also be considered. Generally, the lack of correlation between the loss of mass of galvanized steel and the thickness of the corrosion product formed is due to the high solubility of these products (chlorides and basic sulfates of Zn) in rainwater.

$$CR_{GS} = 2.4320 \times t^{0.8248}\ R^2 = 93.92\% \quad (3)$$

In previous studies for Rapa Nui [58], but in a different area located 300 m from the coastline, a corrosion rate of 3.92 μm $year^{-1}$ was obtained for Zn per year of exposure, classifying as a C4 corrosivity category [30]. By contrast, in studies carried out on the island of Cuba [35] for galvanizing per year of exposure, categories of C4 at 20 m from the coast and C3 at distances ≥4110 m were obtained, with averages of RH 83%, T° 26 °C and $\tau_4$667 h y^{-1}. These were meteorological variable values greater than those obtained in the area located on Easter Island, which were temperatures close to 21 °C, RH 73%, and τ3344 h y^{-1}. Results obtained in the MICAT project for Zn in marine atmospheres S_1P_0 deliver varied values varying between C2 (low) to C4 (high) [58].

3.3. Characterization of corrosion products

3.3.1. Carbon steel

Exposure time naturally generates significant differences in the appearance of carbon steel. Differences observed in this study appear in Fig. 9(a–d), where frontal micrographs and cross-sections are compared with two steels exposed in Rapa Nui for 1 and 3 years.

The micrographs in Fig. 9(a–d) present relatively homogeneous layers of corrosion products, along with fissures which increased markedly from years 1–3. These cracks are generated by the stresses produced in the material when corrosion products are formed, which are greater in volume than their metallic predecessors. Fissures allow the re-entry of chloride and oxygen ions, accelerating corrosion processes. In cross-sectional micrographs (right side), cracks parallel to the steel surface (1 year) are best observed in the corrosion product layer. The crack in the corrosion product generates the takeoff of the corrosion products' upper layer over time, as noted after three years of exposure. This behavior did not occur on the entire surface of the exposed material, though, and did not generate a more significant loss of corrosion product on the steel surface, which does not allude to the occurrence of corrosion by exfoliation. The steel exfoliation process usually occurs at chloride concentrations greater than 300 mg $m^{-2}d^{-1}$, well above the levels found in Rapa Nui for this study. Metallography determined that the corrosion products' thickness after one year was between 120 μm and 140 μm. At three years, these thicknesses varied within a broader range, between 180 μm and 240 μm.

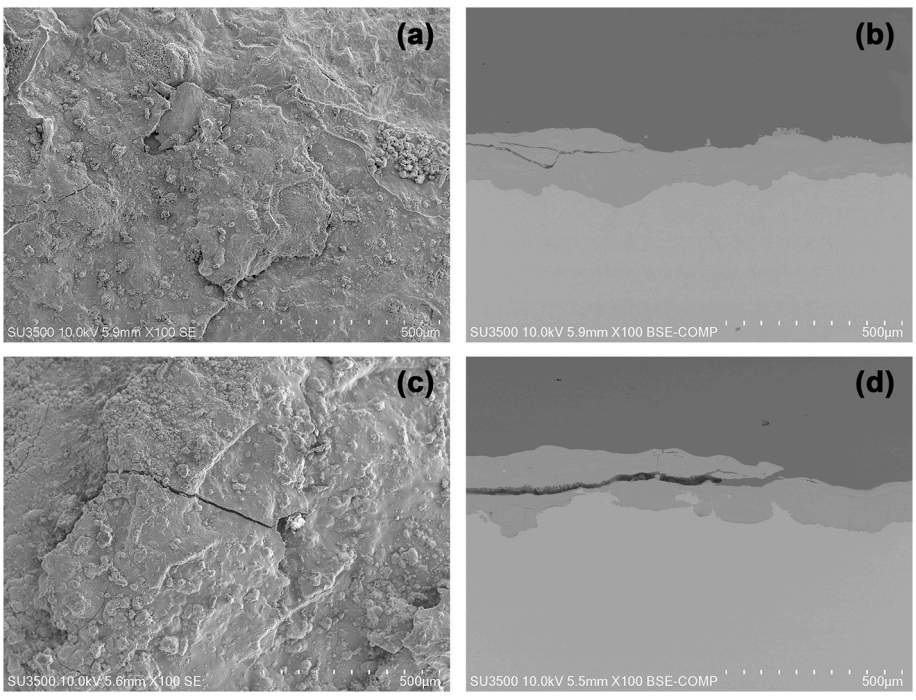

Fig. 9. SEM micrographs of two carbon steels exposed for 1 and 3 years in Rapa Nui (100×). (a–b) surface image and cross-section of the sample after 1 year of exposure, and (c–d) surface image and cross-section of the sample after 3 years of exposure.

Using X-ray diffraction analysis (XRD), we studied the composition of steels' corrosion products in the first and third years of exposure. Several iron hydroxides such as Lepidocrocite and Goethite (γFeOOH and αFeOOH) were identified as main components in the results. Fig. 10a shows DRX results after 3 years. These products are common in marine atmospheres such as Rapa Nui, and have been reported in similar studies [32,38]. In this way, contrary to dry oxidation, the atmospheric corrosion of this material is an electrochemical process that needs aqueous conditions for its occurrence, as mentioned by Hœrlé et al. [61]. This corrosion can be summarized in the stoichiometric equilibrium: 4 Fe (iron substrate) + 3 O_2 (atmosphere) + 2H_2 O (electrolyte) = 4 FeOOH (rust) [61]. In this study, the corrosion products' composition was analyzed using the Raman technique. Spectra analysis was performed by comparing the Raman signals characteristic of synthetic iron oxides and hydroxides reported in the literature [62]. For both exposure periods, six signals centered at 221, 252, 352, 379, 528, and 649 cm^{-1} were identified and assigned to the lepidocrocite phase (γ-FeOOH), a predominant corrosion product on the surface of both samples [61–63]. Identifying this oxyhydroxide alone is consistent with reports of carbon steel exposure to the atmosphere, where the lepidocrocite phase remains virtually pure in the outer layer while the concentration of the goethite phase (α-FeOOH) tends to increase in the inner layer of the corrosion product [62]. The formation of goethite occurs because part of the lepidocrocite and the amorphous ferric oxyhydroxides dissolve due to rainwater, reprecipitating as goethite [62].

3.3.2. Galvanized steel

Fig. 11(a–d) shows the surface and cross-section of two galvanized steels exposed for 1 and 3 years in Rapa Nui. In the micrograph, the exposure year is observed on the surface flat areas of corrosion products. In more localized areas, clusters of corrosion products appear above the surface level. This morphology generally occurs in more active areas of the material, where over time the surface gradually transforms into generalized corrosion, as seen in the micrograph at three years of exposure. In the cutting micrograph (right side), corrosion products are observed that protrude through the level of the material and vary in thickness along the galvanizing, increasing its thickness depending on exposure time (between 5 and 15 μm thick). X-ray Diffraction indicated that in the first year of exposure, the steel has Zincite (ZnO), a common corrosion product of zinc in marine areas with low contaminants [64–69]. Later, after three years of exposure, in addition to zincite, hydrozincite ($Zn(OH)_2$) and simonkolleite ($Zn_5(OH)_8Cl_2$ xH_20) were found. The former is a consequence of marine atmospheres without contaminants, while the latter is where chloride pollution of more than 60 mg m^{-2} d^{-1} of Cl^- promotes simonkolleite formation [27]. Fig. 10 b shows the DRX after 3 years, where the main component is simonkolleite ($Zn_5(OH)_8Cl_2$ xH_20) and the secondary component detected was hydrated zinc carbonate hydroxide.

3.4. Electrochemical measurements

3.4.1. Carbon steel

The protective nature of the corrosion products formed on the steel was studied by tracing anodic polarization curves (oxidation reaction). In this method, the displacement of potential towards more positive values and the displacement of anodic current towards lower values compared to the material without environmental exposure, jointly indicate a barrier effect from the corrosion product layer against oxidation in a solution of 0.1 M Na_2SO_4. Fig. 12 presents the results of the plotted curves, observing a displacement of the initial potential from −650.2 mVecs of unexposed steel to −451.4 mVecs of steel after one year of exposure, and to −343.3 mVecs of steel after three years. A decrease in the anodic current is observed as a function of the exposure time. To quantify current, a constant potential of 100 mVecs was chosen in the three curves, obtaining a current value of 3.62×10^{-2} A cm^{-2} for steel that was not exposed (steel without corrosion, i.e., without compounds that act as a barrier); 4.19×10^{-3} A cm^{-2} for steel exposed for one year; and 4.31×10^{-6} A cm^{-2} for steel exposed for three years. The potential and anodic current results corroborate the formation of a more protective corrosion product layer, which increases its thickness depending on exposure time. The film increases in thickness depending on the

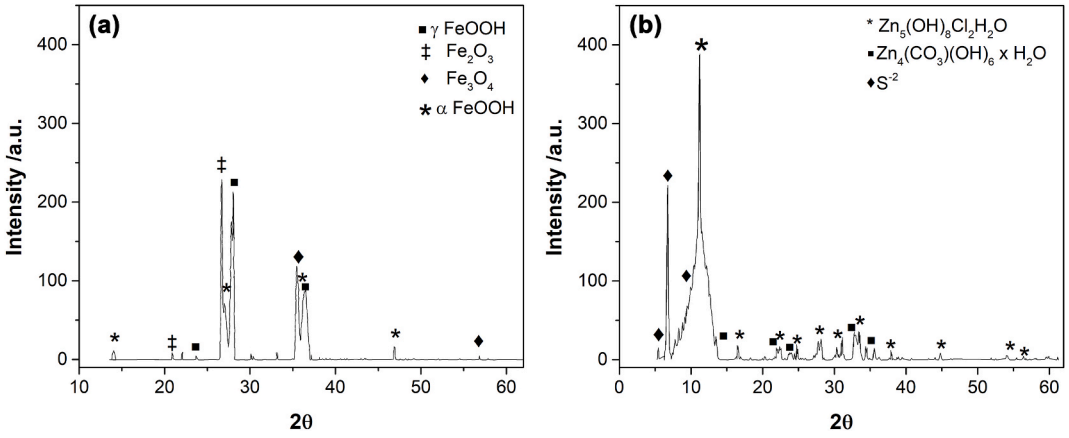

Fig. 10. X-ray diffraction analysis (XRD) of samples after 3 years of exposure time: (a) steel, where the main components were Lepidocrocite and Goethite, (b) galvanized steel, where the main component was simonkolleite.

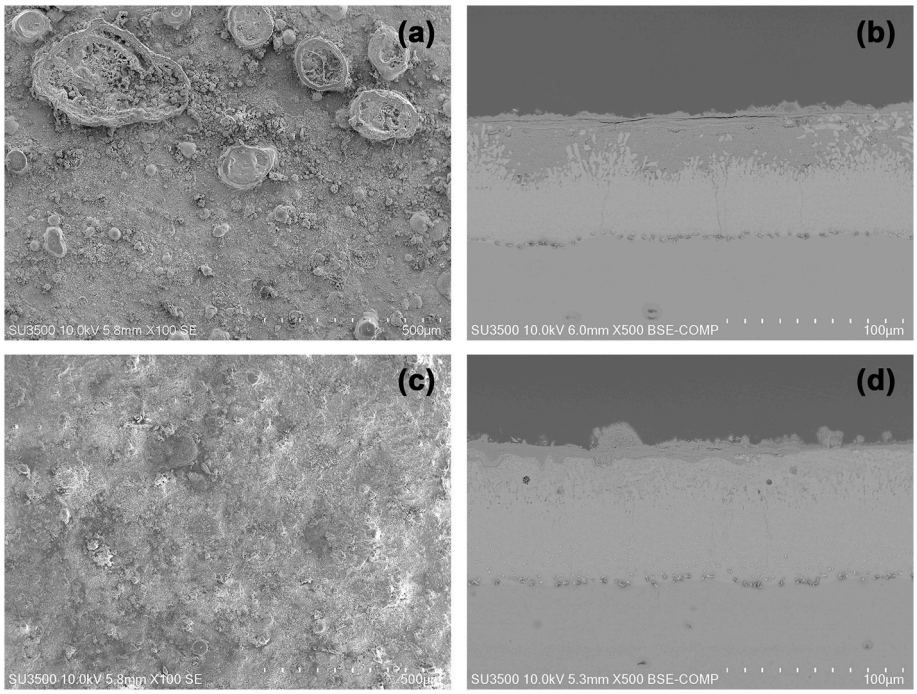

Fig. 11. SEM micrographs of two galvanized steels exposed to the environment on Rapa Nui (100×). (a–b) surface image and cross-section of the sample after 1 year of exposure, and (c–d) surface image and cross-section of the sample after 3 years of exposure.

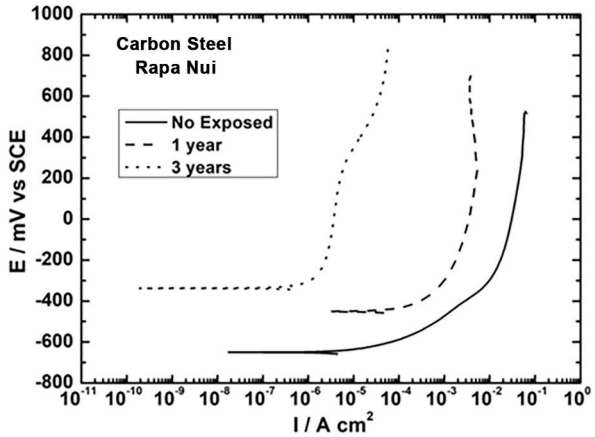

Fig. 12. Anodic curves for unexposed carbon steel, with 1 and 3 years of exposure.

appearance of fissures in the layer, and whether these are connected or if they block entry for the aggressive medium. According to anodic current data, fissures are expected to be unconnected. Goethite formation must also be considered over time. This compound ennobles the layer of corrosion products formed, raising corrosion potential and decreasing the anodic current.

3.4.2. Galvanized steel

Fig. 13 shows the variation in anodic polarization curves obtained for galvanized steel with or without environmental exposure for one and three years. A small potential displacement is observed from −1112.1 mVsce (galvanized without exposure) to −1051.5 mVsce (galvanized exposed to 1 and 3 years), corroborating the formation of the corrosion product. Anodic current displacement towards lower values is observed depending on exposure time, due to the formation of a protective film of corrosion acting as a barrier against the environment. To quantify current, a line was drawn parallel to the x-axis at the potential of −600 mVsce, obtaining current values of 2.52×10^{-2} A cm^{-2} for unexposed galvanized steel, 9.75×10^{-4} A cm^{-2} per year of exposure, and 1.18×10^{-4} A cm^{-2} at three years of exposure. The decrease in the anodic current during the exposure time corroborates the increase in corrosion product thickness at three years of exposure, as shown in Fig. 13.

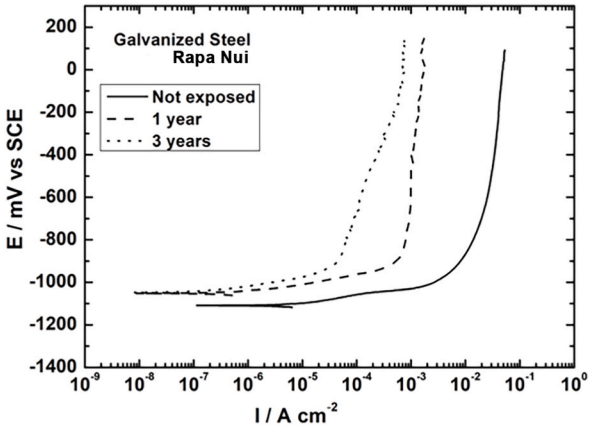

Fig. 13. Anodic polarization curve of unexposed galvanized steel exposed to 1 and 3 years.

3.5. Impact toughness measurements

Mild steels, such as 1020, are materials with high corrosion rates in marine and industrial environments. This has been demonstrated with mechanical properties such as ultimate tensile strength (UTS) and ductility [45]. The strongest effect is on ductility, a property closely related to toughness. These properties are obtained from the tensile test, a quasi-static method, through which the impact toughness can be indirectly determined. In this project, the impact toughness was evaluated with the Charpy, a dynamic evaluation method which lets us directly determine this property.

3.5.1. Carbon steel

Carbon steel is a material that rapidly corrodes when left unprotected, generating corrosion products which will alter its surface. Fig. 14(a–f) illustrates this with corrosion action on a steel surface exposed for 2 years in a C3 environment. In this study, we determined corrosion rate rates with samples exposed on racks (see Fig. 14a and b). Impact toughness test samples were first simultaneously hung out on the racks (Fig. 14 c, d, e and f). As the figures show, the surface aspect of the corrosion products was similar both in the steel exposed on the racks, and in the hanging samples. The fundamental difference between these samples is that the hanging samples faced wind action, which in theory could reduce the samples' moistening time compared to the rack samples, and their movement can vary the exposed and non-exposed zones compared with the fixed exposed face on the rack. There are also moments where the sample face with the fissure directly faces the environment and other moments where it does not, thereby influencing the samples' toughness determination. Average wind speeds in the study zone were 4.40, 4.38 and 4.59 m/s during years 1, 2 and 3 respectively. This situation could effectively make the atmospheric corrosion effect even stronger in the rack samples via this study. The data obtained are an initial measurement, though, offering us reference values that were previously unreported. The results obtained in this study, in terms of impact toughness, for the exposed Charpy samples appear in Fig. 15.

Before being exposed, the steel used in this study showed an average toughness of 63J. However, this property was strongly affected by exposure, as shown in Fig. 15. At only three months of exposure, toughness was reduced to a third. In the following months, it continued to show a much slower decline. Finally, after 36 months, the steel presented 16J on average, which represents 25% of the original value and a considerable loss of toughness for the material.

With the data on corrosion rate and toughness, a graphic comparison was made, shown in Fig. 16. It can be observed that with an adjustment in the scales, there is a relationship between the corrosion rate and the loss of toughness shown by the steel over time. It is important to emphasize that in this study, low-carbon steel was used without any surface protection. This represents an extreme condition for the material without an actual application since it is not typically used in structures. For this reason, the corrosion effects are much greater than what is found in structural steels used in coastal environments. We then show results for galvanized steel, a type of steel found in structural applications. This study and its results show that toughness drops dramatically due to atmospheric corrosion. If this fact is not considered in material design or selection, the material will thus have an unexpectedly fragile design.

3.5.2. Galvanized steel

Galvanizing steel is a robust, durable and cheap protection method [51], and helps with many atmospheric and underground conditions [70]. Galvanized steels are protected by the formation of a protective layer, made of iron and zinc compounds, whose composition varies as a function of distance, as shown in Fig. 17a. After solidification, the coating consists of an outer layer of 100% zinc (η-eta layer) and inner layers called alloy layers consisting of intermetallic phases of iron and zinc such as zeta (ζ) layer (94% Zn–6% Fe), delta (δ) layer (90% Zn–10% Fe), and gamma (Γ) layer (75% Zn–25% Fe) [71] (see Fig. 17b). These compounds' differing composition and structure makes their properties different as well, including their mechanical properties, as we can see in their toughness (HV) [72,73]. The microfissures included in the solidification often occur in galvanized covering, due to the large difference between the thermal expansion coefficients of the zinc covering and the iron substrate. This can influence the density of cracks forming

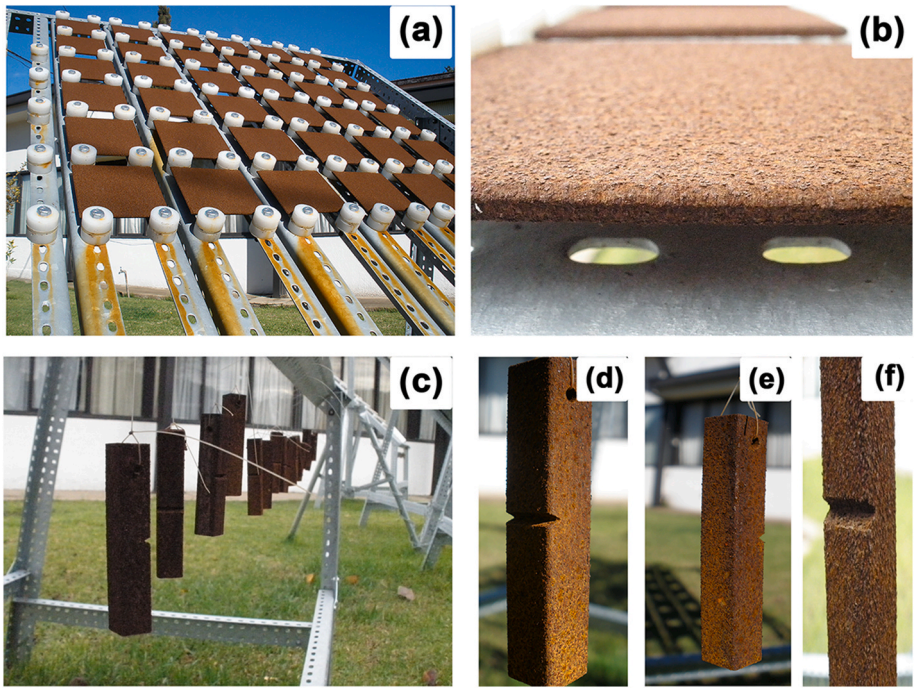

Fig. 14. Photographs of the racks used in the study stations, showing (a–b) the upper section of the rack and the samples exposed to determine corrosion rate, and the hanging samples for impact toughness tests (c–f) after 2 years' exposure in a C3 environment.

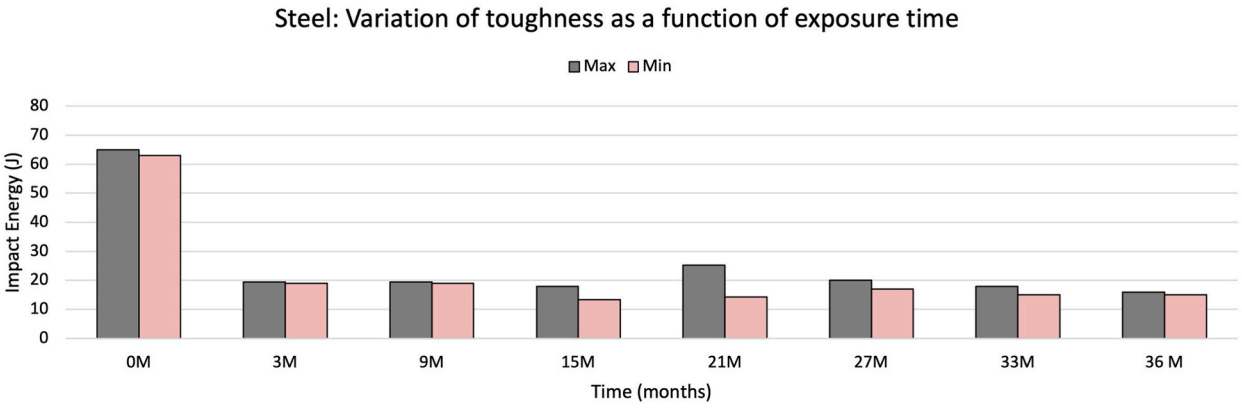

Fig. 15. Steel toughness obtained at different exposure periods.

in the zinc layer, and the subsequent delamination of the covering under weight. The zinc grains show a strong trend towards anisotropic mechanical properties, which in turn influences the deformation and behavior of the zinc layer [74].

In this study, both the samples on racks and the hanging samples used for the impact toughness test were treated with a conventional hot dip galvanizing process. Fig. 18 shows the results of this study, in terms of impact toughness as a function of exposure time.

Conventional hot-dip galvanized steel loses about a third of its toughness due to the formation of a layer of phases different from the original alloy, and because these phases have different toughness levels, all lower than steel [72]. This was demonstrated in this study when the same steel, ungalvanized and without exposure, presented a toughness of 63J, and 20J when galvanized (Figs. 14 and 17). However, our results showed that the low toughness of galvanized steel was affected more slowly than that of unprotected steel. After 36 months, galvanized steel presented 12J on average, representing 63% of the original value, indicating that these steels are more effective in corrosion protection and toughness. As with steel, a visual separation was made with the corrosion rate data and toughness (Fig. 19). A relationship is seen similar to that found in Fig. 16. Therefore, with a scale adjustment, there is an apparent connection between corrosion rate and loss of toughness shown by galvanized steel over time.

The results of this study demonstrate the protective effect of galvanization against corrosion. However, they also show that the

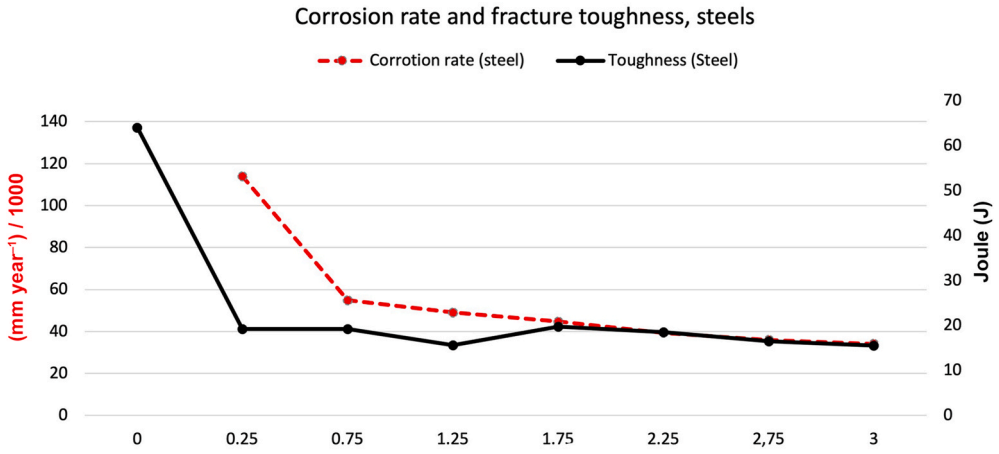

Fig. 16. Graphic comparison between corrosion rate and fracture toughness loss in steels.

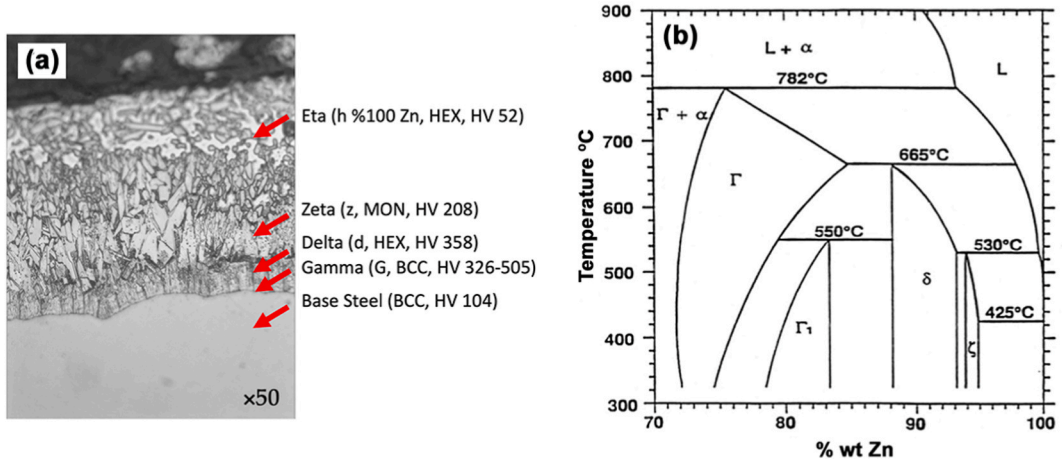

Fig. 17. (a) Microstructure of galvanized steel used in the study, showing the phases composing the galvanized layer, magnified 50×, (b) Zone rich in Zn, of the phase diagram in equilibrium Zn-Fe [73].

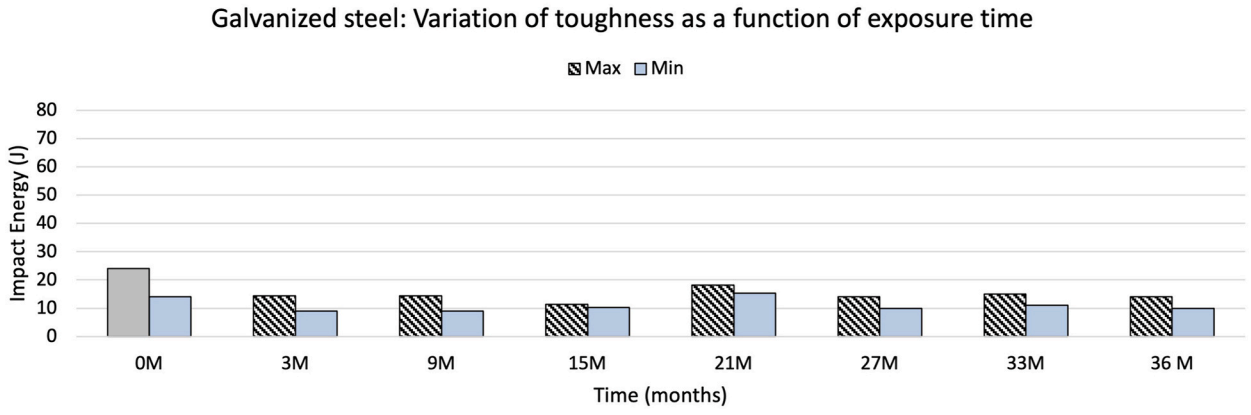

Fig. 18. Toughness of galvanized steels obtained at different exposure periods.

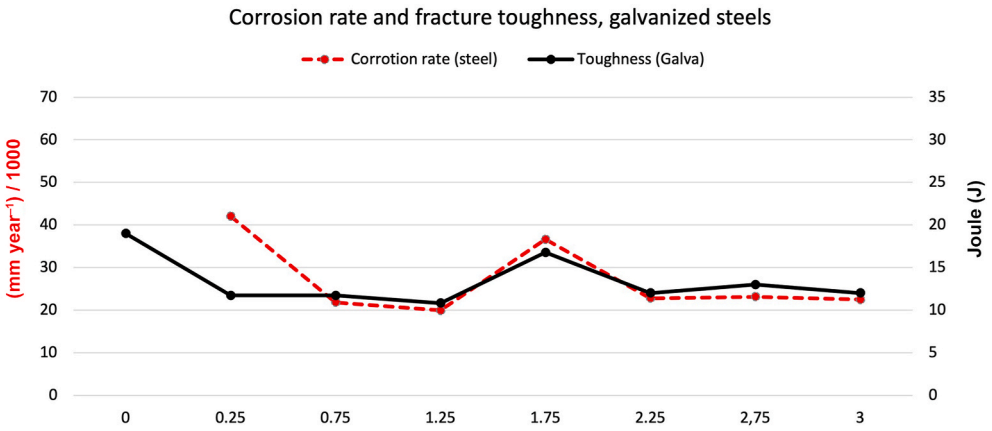

Fig. 19. Graphic comparison between corrosion rate and fracture toughness loss in galvanized steels.

intermetallic compounds which promote this protection reduce the impact toughness of the material. This property is still more stable, for the same exposure time, than in unprotected steels.

4. Conclusions

Both corrosion products and surface deterioration of galvanized and non-galvanized steels promoted lower fracture toughness. Over time, a relationship between corrosion rate and toughness reduction was observed. The corrosion rate and toughness loss were lower in the galvanized steel samples, showing the protective power of this coating type against atmospheric corrosion damage.

In recent decades, alterations of meteoro-chemical variables (climate change and pollutants) have generated difference in materials' behavior against atmospheric corrosion and their subsequent deterioration and lifespan. This in turn influences the protection method to be used against a particularly aggressive medium. The human effect is remarkable in this sense, since the growth reported on the island is related to consumption generating and increasing atmospheric pollutants. This study was carried out on the same island 20 years later (MICAT), with some variations in altitude and distance from the sea, and an environmental SO_2 content three times higher than in previous periods. The corrosion rate of the carbon steel increased 1.5 times; however, the galvanized steel did not increase its corrosion rate. This effect could be related to the layer of zinc compounds that is generated in the galvanized coating, which seems to generate a "barrier effect" preventing the corrosion rate from accelerating, as it did with steel.

The environmental corrosivity categories determined under the conditions of this study were C4 for carbon steel (51.95 μm $year^{-1}$) and C3 for galvanized steel (2.0 μm $year^{-1}$). The average environmental category for three years in this study was t4S1P0.

Corrosion products formed on the carbon steel had Lepidocrocite and Goethite as the main components, and oxides such as magnetite and maghemite as secondary components, which is the same as the findings from 20 years ago in the previous MICAT study. Zincite was formed on the surface of galvanized steel as the main product, with hydrozincite and simonkolleite as secondary products. The by-products of galvanized steel prove that the environment is not rural, but urban.

Author contribution statement

Rosa Vera, Paula Rojas: Conceived and designed the experiments; Performed the experiments; Analyzed and interpreted the data; Contributed reagents, materials, analysis tools or data; Wrote the paper.

Bárbara Valverde, Elizabeth Olave, Rodrigo Sánchez, Andrés Díaz-Gómez, Lisa Muñoz: Analyzed and interpreted the data; Contributed reagents, materials, analysis tools or data.

Funding

This work was supported by Innova-CORFO [Project No 09CN14-5879]; and Fondequip [EQM 160091].

Data availability

The raw data required to reproduce these findings are available to download from http://www.mapadecorrosionatmosfericadechile.cl.

Declaration of competing interest

The authors declare that they have no known competing financial interests or personal relationships that could have appeared to

influence the work reported in this paper

Acknowledgments

The authors gratefully acknowledge Chilean government support through funds from the Innova-CORFO Project No 09CN14-5879, Fondequip EQM 160091, and the Research Department from the Pontificia Universidad Católica de Valparaíso.

References

[1] S.M. Mousavi, N.M. Dinan, S. Ansarifard, O. Sonnentag, Analyzing spatio-temporal patterns in atmospheric carbon dioxide concentration across Iran from 2003 to 2020, Atmos, Environ. Times X. 14 (2022), 100163, https://doi.org/10.1016/j.aeaoa.2022.100163.
[2] H. Singh, N. Feldl, J.E. Kay, A.L. Morrison, Climate sensitivity is sensitive to changes in ocean heat transport, J. Clim. 35 (2022) 2653–2674, https://doi.org/10.1175/JCLI-D-21-0674.1.
[3] S.-I. An, H.-J. Park, S.-K. Kim, J. Shin, S.-W. Yeh, J.-S. Kug, Intensity changes of Indian Ocean dipole mode in a carbon dioxide removal scenario, Npj Clim. Atmos. Sci. 5 (2022) 20, https://doi.org/10.1038/s41612-022-00246-6.
[4] W. Yang, Y. Zhao, Q. Wang, B. Guan, Climate, CO2, and anthropogenic drivers of accelerated vegetation greening in the Haihe River Basin, Rem. Sens. 14 (2022) 268, https://doi.org/10.3390/rs14020268.
[5] Y.-C. Liang, L.M. Polvani, I. Mitevski, Arctic amplification, and its seasonal migration, over a wide range of abrupt CO2 forcing, Npj Clim. Atmos. Sci. 5 (2022) 14, https://doi.org/10.1038/s41612-022-00228-8.
[6] J.J. Santana, A. Ramos, A. Rodriguez-Gonzalez, H.C. Vasconcelos, V. Mena, B.M. Fernández-Pérez, R.M. Souto, Shortcomings of International standard ISO 9223 for the classification, determination, and estimation of atmosphere corrosivities in subtropical archipelagic conditions—the case of the Canary Islands (Spain), Metals (Basel) 9 (2019) 1105, https://doi.org/10.3390/met9101105.
[7] Y. Zhang, B.M. Ayyub, J.F. Fung, Projections of corrosion and deterioration of infrastructure in United States coasts under a changing climate, Resilient Cities Struct. 1 (2022) 98–109, https://doi.org/10.1016/j.rcns.2022.04.004.
[8] D.J. Wuebbles, Climate Science Special Report: 4th US National Climate Assessment, vol. I, 2021, pp. 213–220, https://doi.org/10.1142/9789811213953_0022.
[9] I.G.M. Instituto Geográfico Militar de Chile, Atlas Geográfico para la Educacion, 2019.
[10] F. Bown, A. Rivera, Climate changes and recent glacier behaviour in the Chilean Lake District, Global Planet. Change 59 (2007) 79–86, https://doi.org/10.1016/j.gloplacha.2006.11.015.
[11] J. Massaferro, I. Larocque-Tobler, S.J. Brooks, M. Vandergoes, A. Dieffenbacher-Krall, P. Moreno, Quantifying climate change in Huelmo mire (Chile, Northwestern Patagonia) during the Last Glacial Termination using a newly developed chironomid-based temperature model, Palaeogeogr. Palaeoclimatol. Palaeoecol. 399 (2014) 214–224, https://doi.org/10.1016/j.palaeo.2014.01.013.
[12] C. Muñoz-Mendoza, G. D'Elía, A. Panzera, M.A. Méndez, A. Villalobos-Leiva, J.W. Sites, P.F. Victoriano, Geography and past climate changes have shaped the evolution of a widespread lizard from the Chilean hotspot, Mol. Phylogenet. Evol. 116 (2017) 157–171, https://doi.org/10.1016/j.ympev.2017.08.016.
[13] P. Monsalves-Gavilán, J. Pincheira-Ulbrich, F. Rojo Mendoza, Climate change and its effects on urban spaces in Chile: a summary of research carried out in the period 2000-2012, Atmósfera 26 (2013) 547–566, https://doi.org/10.1016/S0187-6236(13)71095-6.
[14] K. Verichev, M. Zamorano, M. Carpio, Effects of climate change on variations in climatic zones and heating energy consumption of residential buildings in the southern Chile, Energy Build. 215 (2020), 109874, https://doi.org/10.1016/j.enbuild.2020.109874.
[15] N. Blin, M. Hausner, S. Leray, C. Lowry, F. Suárez, Potential impacts of climate change on an aquifer in the arid Altiplano, northern Chile: the case of the protected wetlands of the Salar del Huasco basin, J. Hydrol. Reg. Stud. 39 (2022), 100996, https://doi.org/10.1016/j.ejrh.2022.100996.
[16] R. Vera, D. Delgado, R. Araya, I. Puentes, Mónica, Guerrero, P. Rojas, S. Cabrera, Guillermo Erazo, A.M. Carvajal, Construction of atmospheric corrosion maps in Chile. Preliminary results, Rev. Latinoam. Metal. y Mater. 32 (2012) 269–276.
[17] P. Rojas, C. Martinez, R. Vera, M. Puentes, Toughness of SAE 1020 steel with and without galvanization exposed to different corrosive environments in Chile, Int. J. Electrochem. Sci. 9 (2014) 2848–2858.
[18] R. Vera, M. Puentes, R. Araya, P. Rojas, A. Carvajal, Mapa de corrosión atmosférica de Chile: resultados después de un año de exposición, Rev. La Construcción. 11 (2012) 61–72, https://doi.org/10.4067/S0718-915X2012000200007.
[19] R. Vera, R. Araya, C. Garín, S. Ossandón, P. Rojas, Study on the effect of atmospheric corrosion on mechanical properties with impact test: carbon steel and Galvanized steel, Mater. Corros. 70 (2019) 1151–1161, https://doi.org/10.1002/maco.201810666.
[20] V. Rull, N. Cañellas-Boltà, O. Margalef, A. Sáez, S. Pla-Rabes, S. Giralt, Late Holocene vegetation dynamics and deforestation in Rano Aroi: implications for Easter Island's ecological and cultural history, Quat. Sci. Rev. 126 (2015) 219–226, https://doi.org/10.1016/j.quascirev.2015.09.008.
[21] N. Cañellas-Boltà, V. Rull, A. Sáez, O. Margalef, R. Bao, S. Pla-Rabes, M. Blaauw, B. Valero-Garcés, S. Giralt, Vegetation changes and human settlement of Easter Island during the last millennia: a multiproxy study of the Lake Raraku sediments, Quat. Sci. Rev. 72 (2013) 36–48, https://doi.org/10.1016/j.quascirev.2013.04.004.
[22] V. Rull, N. Cañellas-Boltà, A. Sáez, S. Giralt, S. Pla, O. Margalef, Paleoecology of Easter island: Evidence and uncertainties, Earth Sci. Rev. 99 (2010) 50–60, https://doi.org/10.1016/j.earscirev.2010.02.003.
[23] M. Carvajal, P. Winckler, R. Garreaud, F. Igualt, M. Contreras-López, P. Averil, M. Cisternas, A. Gubler, W.A. Breuer, Extreme sea levels at Rapa Nui (Easter Island) during intense atmospheric rivers, Nat. Hazards 106 (2021) 1619–1637, https://doi.org/10.1007/s11069-020-04462-2.
[24] D.C. Major, P. Blaschke, V. Gornitz, E. Hosek, M. Lehmann, J. Lewis, H. Loehr, G.A. Major-Ex, M. Pedersen Zari, M.J. Vásquez Vargas, E. Watterson, A. Wejs, Adaptation to climate change in small island settlements, Ocean Coast Manag. 212 (2021), 105789, https://doi.org/10.1016/j.ocecoaman.2021.105789.
[25] R.G. Asch, W.W.L. Cheung, G. Reygondeau, Future marine ecosystem drivers, biodiversity, and fisheries maximum catch potential in Pacific Island countries and territories under climate change, Mar. Pol. 88 (2018) 285–294, https://doi.org/10.1016/j.marpol.2017.08.015.
[26] R. Wilts, C. Latka, W. Britz, Who is most vulnerable to climate change induced yield changes? A dynamic long run household analysis in lower income countries, Clim. Risk Manag. 33 (2021), 100330, https://doi.org/10.1016/j.crm.2021.100330.
[27] M. Morcillo, B. Chico, D. de la Fuente, J. Simancas, Looking back on contributions in the field of atmospheric corrosion offered by the MICAT Ibero-American testing Network, Int. J. Corros. 2012 (2012) 1–24, https://doi.org/10.1155/2012/824365.
[28] M. Morcillo, B. Chico, D. de la Fuente, E. Almeida, G. Joseph, S. Rivero, B. Rosales, Atmospheric corrosion of reference metals in Antarctic sites, Cold Reg. Sci. Technol. 40 (2004) 165–178, https://doi.org/10.1016/j.coldregions.2004.06.009.
[29] J. Marco, M. Gracia, J. Gancedo, M. Martın-Luengo, G. Joseph, Characterization of the corrosion products formed on carbon steel after exposure to the open atmosphere in the Antarctic and Easter Island, Corrosion Sci. 42 (2000) 753–771, https://doi.org/10.1016/S0010-938X(99)00090-6.
[30] ISO 9223:2012, Corrosion of Metals and Alloys. Corrosivity of Atmospheres. Classification, Determination and Estimation, 2008, 0–20.
[31] J. Morales, F. Díaz, J. Hernández-Borges, S. González, V. Cano, Atmospheric corrosion in subtropical areas: statistic study of the corrosion of zinc plates exposed to several atmospheres in the province of Santa Cruz de Tenerife (Canary Islands, Spain), Corrosion Sci. 49 (2007) 526–541, https://doi.org/10.1016/j.corsci.2006.04.023.
[32] J. Santana Rodrıguez, F. Santana Hernández, J. González González, XRD and SEM studies of the layer of corrosion products for carbon steel in various different environments in the province of Las Palmas (The Canary Islands, Spain), Corrosion Sci. 44 (2002) 2425–2438, https://doi.org/10.1016/S0010-938X(02)00047-1.
[33] L. Núñez, E. Reguera, F. Corvo, E. González, C. Vazquez, Corrosion of copper in seawater and its aerosols in a tropical island, Corrosion Sci. 47 (2005) 461–484, https://doi.org/10.1016/j.corsci.2004.05.015.

[34] J. Morales, F. Díaz, J. Hernández-Borges, S. González, Atmospheric corrosion in subtropical areas: XRD and electrochemical study of zinc atmospheric corrosion products in the province of Santa Cruz de Tenerife (Canary Islands, Spain), Corrosion Sci. 48 (2006) 361–371, https://doi.org/10.1016/j.corsci.2005.02.030.

[35] A. Castañeda, C. Valdés, F. Corvo, Atmospheric corrosion study in a harbor located in a tropical island, Mater. Corros. 69 (2018) 1462–1477, https://doi.org/10.1002/maco.201810161.

[36] X. Lu, Y.-W. Liu, H. Zhao, C. Pan, Z. Wang, H. Zhao, C. Pan, Z. Wang, Corrosion behavior of copper in extremely harsh marine atmosphere in Nansha Islands, China, Trans. Nonferrous Metals Soc. China 31 (2021) 703–714, https://doi.org/10.1016/S1003-6326(21)65531-0.

[37] C. Peng, Y. Liu, M. Guo, T. Gu, C. Wang, Z. Wang, C. Sun, Corrosion and pitting behavior of pure aluminum 1060 exposed to Nansha Islands tropical marine atmosphere, Trans. Nonferrous Metals Soc. China 32 (2022) 448–460, https://doi.org/10.1016/S1003-6326(22)65806-0.

[38] Y. Liu, Corrosion behavior of low-carbon steel and weathering steel in a coastal zone of the spratly islands: a tropical marine atmosphere, Int. J. Electrochem. Sci. (2020) 6464–6477, https://doi.org/10.20964/2020.07.48.

[39] C. Titakis, P. Vassiliou, Evaluation of 4-year atmospheric corrosion of carbon steel, aluminum, copper and zinc in a Coastal Military Airport in Greece, Corros. Mater. Degrad. 1 (2020) 159–186, https://doi.org/10.3390/cmd1010008.

[40] P.R. Roberge, R.D. Klassen, P.W. Haberecht, Atmospheric corrosivity modeling — a review, Mater. Des. 23 (2002) 321–330, https://doi.org/10.1016/S0261-3069(01)00051-6.

[41] I.T. Fonseca, R. Picciochi, M. Mendonça, A. Ramos, The atmospheric corrosion of copper at two sites in Portugal: a comparative study, Corrosion Sci. 46 (2004) 547–561, https://doi.org/10.1016/S0010-938X(03)00176-8.

[42] F. Vidal, R. Vicente, J. Mendes Silva, Review of environmental and air pollution impacts on built heritage: 10 questions on corrosion and soiling effects for urban intervention, J. Cult. Herit. 37 (2019) 273–295, https://doi.org/10.1016/j.culher.2018.11.006.

[43] Y. Fan, W. Liu, S. Li, T. Chowwanonthapunya, B. Wongpat, Y. Zhao, B. Dong, T. Zhang, X. Li, Evolution of rust layers on carbon steel and weathering steel in high humidity and heat marine atmospheric corrosion, J. Mater. Sci. Technol. 39 (2020) 190–199, https://doi.org/10.1016/j.jmst.2019.07.054.

[44] J.G. Castaño, C.A. Botero, S. Peñaranda, A review of the atmospheric corrosion of zinc in outdoor and indoor atmospheres, Rev. Metal. (Madr.) 43 (2007), https://doi.org/10.3989/revmetalm.2007.v43.i2.60.

[45] C. Martínez, F. Briones, M. Villarroel, R. Vera, Effect of atmospheric corrosion on the mechanical properties of SAE 1020 structural steel, Materials (Basel) 11 (2018) 591, https://doi.org/10.3390/ma11040591.

[46] E.-98 ASTM, Standard Test Methods for Notched Bar Impact Testing of Metallic Materials, Philadelphia, 2012.

[47] A. Dolzhenko, R. Kaibyshev, A. Belyakov, Tempforming as an advanced processing method for carbon steels, Metals (Basel) 10 (2020) 1566, https://doi.org/10.3390/met10121566.

[48] A. Rosenauer, D. Brandl, G. Ressel, S. Lukas, S. Monschein, M. Stockinger, R. Schnitzer, Influence of delta ferrite on the impact toughness of a PH 13-8 Mo maraging steel, Mater. Sci. Eng. 856 (2022), 144024, https://doi.org/10.1016/j.msea.2022.144024.

[49] S. Gao, J. Li, L. Guo, Q. Bai, F. Li, Mechanical properties and low-temperature impact toughness of high-strength bolts after elevated temperatures, J. Build. Eng. 57 (2022), 104851, https://doi.org/10.1016/j.jobe.2022.104851.

[50] S. Aden-Ali, A. Chamat, J. Gilgert, E.J. Petit, S. Dominiak, L. Schmitt, M. Gilles, Z. Azari, On the degradation the endurance of silicon-rich TRIP800 steel after hot-dip galvanization, Eng. Fail. Anal. 16 (2009) 2009–2019, https://doi.org/10.1016/j.engfailanal.2009.04.001.

[51] O. Joseph, J. Olakunle, D. Joseph, A. Odedeji, Corrosion resistance of galvanized roofing sheets in acidic and rainwater environments, Heliyon 7 (2021), e08647, https://doi.org/10.1016/j.heliyon.2021.e08647.

[52] R. Vera, B. Valverde, E. Olave, A. Díaz-Gómez, R. Sánchez-González, L. Muñoz, C. Martínez, P. Rojas, Corrosion behavior of copper exposed in marine tropical atmosphere in Rapa Nui (Easter Island) Chile 20 Years after MICAT, Metals (Basel) 12 (2022), https://doi.org/10.3390/met12122082, 2082.

[53] ISO 9224:2012, Corrosion of Metals and Alloys - Corrosivity of Atmospheres - Guiding Values for the Corrosivity Categories, 2012. www.aenor.es.

[54] ISO 9225:2012, Corrosivity of Atmospheres - Measurement of Environmental Parameters Affecting Corrosivity of Atmospheres, 2012. www.aenor.es.

[55] ISO 9226:2012, Corrosion of Metals and Alloys - Corrosivity of Atmospheres - Determination of Corrosion Rate of Standard Specimens for the Evaluation of Corrosivity, 2012. www.aenor.es.

[56] ASTM G1 − 03, Standard Practice for Preparing, Cleaning, and Evaluating Corrosion Test Specimens, in: ASTM Spec. Tech. Publ, i, 2017, pp. 505–510, https://doi.org/10.1520/G0001-03R17E01.2.

[57] ASTM G50-20, G50 -Standard Practice for Conducting Atmospheric Corrosion Tests on Metals, vol. 1, ASTM Copyright, 2020, pp. 1–6, https://doi.org/10.1520/G0050-20.2.

[58] M. Morcillo, E. Almeida, B. Rosales, J. Uruchurtu, M. Marrocos, Corrosion y proteccion de metales en las atmosferas de Iberoamerica, Parte I, CYTED, 1998.

[59] K. Routledge, Anu. Isla de Pascua, Hidrogr. Mar. Chile, 1916, pp. 374–393.

[60] Y.M. Panchenko, A.I. Marshakov, T.N. Igonin, V.V. Kovtanyuk, L.A. Nikolaeva, Long-term forecast of corrosion mass losses of technically important metals in various world regions using a power function, Corrosion Sci. 88 (2014) 306–316, https://doi.org/10.1016/j.corsci.2014.07.049.

[61] S. Hœrlé, F. Mazaudier, P. Dillmann, G. Santarini, Advances in understanding atmospheric corrosion of iron. II. Mechanistic modelling of wet–dry cycles, Corrosion Sci. 46 (2004) 1431–1465, https://doi.org/10.1016/j.corsci.2003.09.028.

[62] J. Alcántara, B. Chico, J. Simancas, I. Díaz, D. de la Fuente, M. Morcillo, An attempt to classify the morphologies presented by different rust phases formed during the exposure of carbon steel to marine atmospheres, Mater. Char. 118 (2016) 65–78, https://doi.org/10.1016/j.matchar.2016.04.027.

[63] W. Kiefer, Recent Advances in linear and nonlinear Raman spectroscopy I, J. Raman Spectrosc. 38 (2007) 1538–1553, https://doi.org/10.1002/jrs.1902.

[64] A.K. Sinha, A. Anand, Development of an alternative for corrosive resistant galvanized steel compatible for laser welding, Mater. Today Proc. 46 (2021) 9561–9563, https://doi.org/10.1016/j.matpr.2020.04.096.

[65] E.J. Petit, Y. Grosbety, S. Aden-Ali, J. Gilgert, Z. Azari, Microstructure of the coating and mechanical properties of galvanized chromium-rich martensitic steel, Surf. Coating. Technol. 205 (2010) 2404–2411, https://doi.org/10.1016/j.surfcoat.2010.09.032.

[66] D. de la Fuente, I. Díaz, J. Simancas, B. Chico, M. Morcillo, Long-term atmospheric corrosion of mild steel, Corrosion Sci. 53 (2011) 604–617, https://doi.org/10.1016/j.corsci.2010.10.007.

[67] A. Kaleva, T. Tassaing, V. Saarimaa, G. Le Bourdon, P. Väisänen, A. Markkula, E. Levänen, Formation of corrosion products on zinc in wet supercritical and subcritical CO2: in-situ spectroscopic study, Corrosion Sci. 174 (2020), 108850, https://doi.org/10.1016/j.corsci.2020.108850.

[68] Y. Meng, L. Liu, D. Zhang, C. Dong, Y. Yan, A.A. Volinsky, L.-N. Wang, Initial formation of corrosion products on pure zinc in saline solution, Bioact. Mater. 4 (2019) 87–96, https://doi.org/10.1016/j.bioactmat.2018.08.003.

[69] S. Li, L.H. Hihara, Aerosol salt Particle deposition on metals exposed to marine environments: a study related to marine atmospheric corrosion, J. Electrochem. Soc. 161 (2014) C268–C275, https://doi.org/10.1149/2.071405jes.

[70] D. Nakhaie, A. Kosari, J.M.C. Mol, E. Asselin, Corrosion resistance of hot-dip galvanized steel in simulated soil solution: a factorial design and pit chemistry study, Corrosion Sci. 164 (2020), 108310, https://doi.org/10.1016/j.corsci.2019.108310.

[71] S.M.A. Shibli, B.N. Meena, R. Remya, A review on recent approaches in the field of hot dip zinc galvanizing process, Surf. Coating. Technol. 262 (2015) 210–215, https://doi.org/10.1016/j.surfcoat.2014.12.054.

[72] H. Inui, N.L. Okamoto, S. Yamaguchi, Crystal structures and mechanical properties of Fe–Zn intermetallic compounds formed in the coating layer of Galvannealed steels, ISIJ Int. 58 (2018) 1550–1561, https://doi.org/10.2355/isijinternational.ISIJINT-2018-066.

[73] A. Chakraborty, R. Ghosh, M. Sudan, A. Mondal, Improvement in hot dip galvanized coating microstructure and properties by pre-metallic deposition on steel surface: a comprehensive review, Surf. Coating. Technol. 449 (2022), 128972, https://doi.org/10.1016/j.surfcoat.2022.128972.

[74] Y. Rico Oviedo, E.J. Carrasquero Rodríguez, Efecto de la composición química en el comportamiento mecánico de recubrimientos galvanizados por inmersión en caliente: una revisión, Ingenius 30 (2017), https://doi.org/10.17163/ings.n18.2017.04.